The Meshless Local Boundary Equation Method

B. Honarbakhsh[1] and A. Tavakoli[1, 2]

[1]Department of Electrical Engineering
[2]Institute of Communications Technology and Applied Electromagnetics
Amirkabir University of Technology (Tehran Polytechnic), Tehran, IRAN
b_honarbakhsh@aut.ac.ir, tavakoli@aut.ac.ir

Abstract ─ A method similar to the local boundary integral equation method that preserves its properties and is free from singular integrals is proposed. The approach is based on selection of the weighting functions from a homogeneous solution of the problem rather than the fundamental solution. Many examples of 2D Laplace and Helmholtz equations and 3D vector wave equation are presented for verification. The method shows optimistic performance over piece-wise smooth boundaries. Radial basis functions of thin plate spline type are used for meshless discretization. The dependable performance of the proposed method provides a hopeful applicability to numerical solutions of partial differential equations.

Index Terms ─ Helmholtz, Laplace, meshless, vector wave equation.

I. INTRODUCTION

Recently, meshless methods have become an attractive research area for electrical engineers [1-19]. In its evolution, one can recognize three turning points. First, the development of the meshless local Petrov-Galerkin (MLPG) method that removes the entire-domain integration leading to computational efficiency [20]. Second, the development of the local boundary integral equation (LBIE) method that not only makes imposing the Dirichlet (essential) boundary condition (EBC) with a weak form of the problem possible, but also reduces the computational cost [21]. Third, the construction of the multi-dimensional interpolation functions (interpolants) with non-singular moment matrix that simplifies the imposition of essential boundary conditions (EBCs) [22].

Since the weighting function in the LBIE is constructed from the fundamental solution of the problem, singular integrands appear at the boundary nodes. Obviously, the order of the singularity of the aforementioned weighting function (companion solution) depends on the differential operator and the dimension of the problem. For example, the companion solution of a 2D Laplace equation is weak singular and is hyper-singular for a 3D vector wave equation. Consequently, numerical implementation of the LBIE is not as straightforward as other meshfree methods. Therefore, a method that has the same valuable properties of the LBIE but is free from singular integrands is desirable.

The main purpose of this paper is to suggest an approach that could circumvent the singular integrands. Our approach is based on selection of the weighting functions from a homogeneous solution of the problem, which is in general, a well-behaved function. Inspired by the well-known MLPG, we call this method meshless local boundary equation (MLBE). In MLPG, the local form of the Petrov-Galerkin statement of the problem is discretized by meshless shape functions. Similarly, in MLBE, the local form of the proposed boundary equation governing the problem is discretized by meshless shape functions.

We applied the method to a number of abstract examples including Laplace, Helmholtz and vector wave equations, all with piece-wise smooth boundaries. We have also verified the two important capabilities of the meshfree methods, i.e., their robustness in dealing with irregular node arrangements and their flexibility in hybridization.

Submitted On: Feb. 8, 2012
Accepted On: April 28, 2012

II. THE BOUNDARY EQUATION

Consider the following two-dimensional second-order boundary value problem (BVP):

$$\begin{cases} \nabla^2 u(\mathbf{x}) + k_0^2 u(\mathbf{x}) = p(\mathbf{x}), & \mathbf{x} \in \Omega \\ u = \bar{u}, & \mathbf{x} \in \Gamma_u \\ u_{,n} + \xi u = \bar{q}, & \mathbf{x} \in \Gamma_q \end{cases} . \tag{1}$$

Where Ω is the problem domain and $\partial\Omega \equiv \Gamma = \Gamma_u \bigcup \Gamma_q$ is the problem boundary. With the above definition, four different problems can be formulated, which are named P1 through P4 as follows:

$$\begin{cases} k_0 = 0 \begin{cases} p = 0 & (\mathrm{P1}) \\ p \neq 0 & (\mathrm{P2}) \end{cases} \\ k_0 \neq 0 \begin{cases} p = 0, (\bar{u} \vee \bar{q}) \neq 0 \\ p \neq 0 \end{cases} (\mathrm{P3}) \\ \qquad\quad p = 0, (\bar{u} \wedge \bar{q}) = 0 \quad (\mathrm{P4}) \end{cases} . \tag{2}$$

Where P1, P2 and P3 are Laplace, Poisson and Helmholtz equations respectively. P4 is a Helmholtz eigenvalue problem. Since the first three of the above are different in nature from the last, we will split this part to two sections and discuss each case separately.

A. Boundary equation for P1-P3

Following the method of weighted residuals [23], one can seek the solution of these cases by considering the following weighted integral:

$$\int_\Omega w\left(\nabla^2 u + k_0^2 u - p\right) d\Omega = 0. \tag{3}$$

Where *w* is the weighting function. Applying the scalar Green's theorem to (3) results in an equivalent weak formulation of the original problem:

$$\int_\Omega u\left(\nabla^2 w + k_0^2 w\right) d\Omega + \int_\Gamma \left(w u_{,n} - w_{,n} u\right) d\Gamma - \int_\Omega w p d\Omega = 0. \tag{4}$$

Imposing the boundary conditions leads to:

$$\begin{aligned} &\int_\Omega u\left(\nabla^2 w + k_0^2 w\right) d\Omega + \int_{\Gamma_u} w u_{,n} d\Gamma - \int_{\Gamma_q} \left(w\xi + w_{,n}\right) u d\Gamma \\ &= \int_\Omega w p d\Omega + \int_{\Gamma_u} w_{,n} \bar{u} d\Gamma - \int_{\Gamma_q} w \bar{q} d\Gamma. \end{aligned} \tag{5}$$

By a proper choice of *w*, the domain (surface for 2D and volume for 3D problems) integral of the left hand side could be eliminated. Obviously, there exist at least two possibilities. First, *w* is the fundamental solution of the main problem. Here, *w* is unique and will lead to the boundary integral equation (BIE) introduced in [21]:

$$\begin{aligned} &u(\mathbf{y}) + \int_{\Gamma_u} w u_{,n} d\Gamma - \int_{\Gamma_q} \left(w\xi + w_{,n}\right) u d\Gamma \\ &= \int_\Omega w p d\Omega + \int_{\Gamma_u} w_{,n} \bar{u} d\Gamma - \int_{\Gamma_q} w \bar{q} d\Gamma. \end{aligned} \tag{6}$$

Second, *w* is a homogeneous solution of the main problem. Such a weight function is not unique and leads to our developed boundary equation (BE):

$$\begin{aligned} &\int_{\Gamma_u} w u_{,n} d\Gamma - \int_{\Gamma_q} \left(w\xi + w_{,n}\right) u d\Gamma \\ &= \int_\Omega w p d\Omega + \int_{\Gamma_u} w_{,n} \bar{u} d\Gamma - \int_{\Gamma_q} w \bar{q} d\Gamma. \end{aligned} \tag{7}$$

Both methods have two important features. First, they make it possible to generate the coefficient (stiffness) matrix with (m-1)-dimensional integrals for m-dimensional problems. Second, the EBCs can be imposed by the weak statement directly. On the other hand, both methods suffer from one difficulty. In the BIE, the integrands of the boundary integrals are singular since w is made from the Green's function; and in the BE, it is not easy to find a proper homogeneous solution. The second and third integrals of the right hand side of (7) impose the boundary conditions. Being proper is assured only if:

$$\begin{cases} w \neq 0, & \mathbf{x} \in \Gamma_q \\ w_{,n} \neq 0, & \mathbf{x} \in \Gamma_u \end{cases} . \tag{8}$$

Together, they put a sever restriction on choosing a homogeneous solution of the problem. Finding a proper homogeneous solution is an open problem. Of course, we have found one such solution for Laplace, Helmholtz and 3D vector wave equations, admitting that they may not be the best. We anticipate that the convergence rate and accuracy of the method could be improved by other solutions.

B. Boundary equation for P4

This is the most interesting case and is discussed in more detail. The mathematical description of the problem is:

$$\begin{cases} \nabla^2 u(\mathbf{x}) = -k_0^2 u(\mathbf{x}), & \mathbf{x} \in \Omega \\ u = 0, & \mathbf{x} \in \Gamma_u \\ u_{,n} + \xi u = 0, & \mathbf{x} \in \Gamma_q \end{cases} . \tag{9}$$

With k_0 and u as unknowns. Based on [23], the BE solution of the above follows: first, multiply both sides of the Eigen-equation by a weighting function w and integrate over Ω:

$$\int_{\Omega} w\nabla^2 u d\Omega = -k_0^2 \int_{\Omega} wud\Omega. \tag{10}$$

Second, construct the weak form of the left hand side of (10) and impose the boundary conditions. In BE, it is carried out by applying the scalar Green's theorem and leads to:

$$\int_{\Omega} u\nabla^2 w d\Omega + \int_{\Gamma_u} wu_{,n} d\Gamma - \int_{\Gamma_q} \left(w\xi + w_{,n}\right) u d\Gamma = -k_0^2 \int_{\Omega} wud\Omega. \tag{11}$$

Third, choose w to be a proper homogeneous solution of the Laplace equations. This simplifies (11) to:

$$\int_{\Gamma_u} wu_{,n} d\Gamma - \int_{\Gamma_q} \left(w\xi + w_{,n}\right) u d\Gamma = -k_0^2 \int_{\Omega} wud\Omega. \tag{12}$$

Fourth, discretize (12). This step *maps* the main continuous operator eigenvalue equation to a generalized matrix eigenvalue problem. Finally, solve the resulting generalized eigenvalue problem.

III. PROPER HOMOGENEOUS SOLUTIONS

A. Laplace/Poisson equation

In this case, the proper homogeneous solution corresponding to the i^{th} node should satisfy:

$$\begin{cases} \nabla^2 w_i(\mathbf{x}) = 0 \\ w_i(\mathbf{x}) \neq 0,\ \mathbf{x}_i \in \Gamma_q \\ w_{i,n}(\mathbf{x}) \neq 0,\ \mathbf{x}_i \in \Gamma_u \end{cases}. \tag{13}$$

Therefore, one such solution is:

$$w_i(\mathbf{x} + \mathbf{x}_i) = 1 + (\alpha_i x + \beta_i y) + xy. \tag{14}$$

which is a linear combination of three harmonic functions and α_i and β_i are non-zero constant scalar. The above solution is proper because:

$$\begin{cases} w_i(\mathbf{x}_i) = 1 \neq 0 \\ w_{i,x}(\mathbf{x}_i) = \alpha_i \neq 0. \\ w_{i,y}(\mathbf{x}_i) = \beta_i \neq 0 \end{cases} \tag{15}$$

Although for arbitrary shaped boundary, the first of (15) is sufficient for imposing the derivative boundary condition, imposition of Dirichlet type needs non-zero $w_{i,n}$. Suppose n_x and n_y be the Cartesian components of unit normal to Γ. Noting that $w_{i,n} = \alpha_i n_x + \beta_i n_y$, for any curvature α_i and β_i can be selected such that $w_{i,n} \neq 0$.

B. Helmholtz equation

Similarly, the proper homogeneous solution corresponding to the i^{th} node should satisfy:

$$\begin{cases} \nabla^2 w_i(\mathbf{x}) + k_0^2 w_i(\mathbf{x}) = 0 \\ w_i(\mathbf{x}) \neq 0,\ \mathbf{x}_i \in \Gamma_q \\ w_{i,n}(\mathbf{x}) \neq 0,\ \mathbf{x}_i \in \Gamma_u \end{cases}. \tag{16}$$

Thus, one proper solution is:

$$w_i(\mathbf{x} + \mathbf{x}_i) = \sin(\alpha_i x + \beta_i y + \pi/4). \tag{17}$$

Where $\alpha_i^2 + \beta_i^2 = k_0^2$. The above solution is proper because:

$$\begin{cases} w_i(\mathbf{x}_i) = \sin(\pi/4) \neq 0 \\ w_{i,x}(\mathbf{x}_i) = \alpha_i \cos(\pi/4) \neq 0. \\ w_{i,y}(\mathbf{x}_i) = \beta_i \cos(\pi/4) \neq 0 \end{cases} \tag{18}$$

For Cartesian problems both of Laplace and Helmholtz equations can be solved using the aforementioned scalars such that the most symmetric form of the weights results; i.e., $\alpha_i = \beta_i = 1$ for Laplace and $\alpha_i = \beta_i = k_0/\sqrt{2}$ for Helmholtz equation. To explain that a nonzero weigh function and its normal derivative at their local coordinate origin are sufficient, consider that satisfactory results are obtained by local domains with radii much smaller than the average nodal spacing [21]. Thus, the variations of the weight functions over the integration limits are tolerable. The validity of this argument is shown by examples in the paper.

IV. THE LOCAL BOUNDARY EQUATION

In this section, we apply (7), which is a global form to local domains of Ω and generate the local boundary equation (LBE) for P1 through P3. Generalization to P4 is straightforward. Based on the existence of an intersection between the boundaries of a local domain, $\partial\Omega_s$ with the global boundary of the problem Γ, two situations are distinguished (see Fig. 1):

A. Non-intersecting boundaries $\left(\partial\Omega_s \bigcap \Gamma = \varnothing\right)$

In this case, the local form becomes:

$$\int_{\partial\Omega_s}\left(wu_{,n}-w_{,n}u\right)d\Gamma=\int_{\Omega_s}wpd\Omega. \tag{19}$$

B. Intersecting boundaries $\left(\partial\Omega_s\cap\Gamma=\Gamma_s\right)$

The boundary of the local domain is decomposed into two parts, L_s is located completely in Ω without an intersection with Γ, and the other, Γ_s intersects Γ. Therefore, (7) becomes:

$$\int_{L_s}\left(wu_{,n}-w_{,n}u\right)d\Gamma+\int_{\Gamma_s\cap\Gamma_u}wu_{,n}d\Gamma-\int_{\Gamma_s\cap\Gamma_q}\left(w\xi+w_{,n}\right)ud\Gamma$$
$$=\int_{\Omega_s}wpd\Omega+\int_{\Gamma_s\cap\Gamma_u}w_{,n}\bar{u}d\Gamma-\int_{\Gamma_s\cap\Gamma_q}w\bar{q}d\Gamma. \tag{20}$$

This completes the formulation of the LBE method. The remainder is discretization of the local form that maps either (19) or (20) to a system of linear equations. For this purpose, meshless shape functions are used.

V. SHAPE FUNCTION GENERATION

There exist two types of shape functions in meshless literature: approximants and interpolants. Approximants have a longer history than interpolants. Each one has its advantages and disadvantages. There are a number of strategies in generating each also [24]. Here, we have employed radial basis function (RBF) interpolants. Suppose the problem domain, Ω is described by *N* nodes. RBF shape functions interpolate the function *u* by a linear combination of *N* radial functions φ_i, $i=1,...,N$, at any point of Ω. Thus:

$$u^h(\mathbf{x})=\boldsymbol{\Phi}^T(\mathbf{x})\cdot\hat{\mathbf{u}}=\sum_{i=1}^{N}\varphi_i(\mathbf{x})\hat{u}_i. \tag{21}$$

in which $\hat{\mathbf{u}}=\left[\hat{u}_1\ \ ...\ \ \hat{u}_N\right]^T$ and u^h is the RBF interpolation of *u*; therefore, $u^h(\mathbf{x}_i)\equiv u_i=\hat{u}_i$. If the shape functions were approximants, then $u^h(\mathbf{x}_i)\equiv u_i\neq\hat{u}_i$. The coefficient vector $\hat{\mathbf{u}}$ is found by collocating (21) at the nodes. In this paper, φ_i is taken to be 9th and 5th order thin plate spline (TPS) function for 2D and 3D problems.

VI. MESHLESS DISCRETIZATION

For meshless discretization, the unknown function *u* in the final local form, i.e. (19) and (20) should be replaced by its equivalent expression, i.e. (21). Therefore:

$$\mathbf{K}\hat{\mathbf{u}}=\mathbf{f}. \tag{22}$$

with $\hat{\mathbf{u}}$ as unknowns, and entries of $\mathbf{K}$ and $\mathbf{f}$ are given by:

$$f_i=\begin{cases}\int_{\Omega_{si}}w_i pd\Omega\ ,\ \partial\Omega_{si}\cap\Gamma=\varnothing\\ \int_{\Omega_{si}}w_i pd\Omega+\int_{\Gamma_{si}\cap\Gamma_u}w_{i,n}\bar{u}d\Gamma-\int_{\Gamma_{si}\cap\Gamma_q}w_i\bar{q}d\Gamma\ ,\ \partial\Omega_{si}\cap\Gamma=\Gamma_{si}\end{cases}. \tag{23}$$

and:

$$K_{ij}=\begin{cases}\int_{\partial\Omega_{si}}\left(w_i\varphi_{j,n}-w_{i,n}\varphi_j\right)d\Gamma\\ ,\partial\Omega_{si}\cap\Gamma=\varnothing\\ \int_{L_{si}}\left(w_i\varphi_{j,n}-w_{i,n}\varphi_j\right)d\Gamma+\int_{\Gamma_{si}\cap\Gamma_u}w\varphi_{j,n}d\Gamma\\ \qquad-\int_{\Gamma_{si}\cap\Gamma_q}\left(w\xi+w_{,n}\right)\varphi_j d\Gamma\\ ,\partial\Omega_{si}\cap\Gamma=\Gamma_{si}.\end{cases} \tag{24}$$

Once $\hat{\mathbf{u}}$ is computed, the unknown function can be approximated/interpolated at any point of the problem domain.

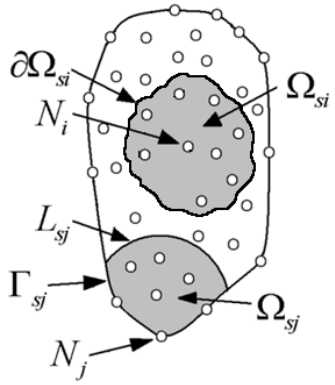

Fig. 1. Nodal geometry description of the problem and necessary definitions for meshless discretization. N_i: i^{th} node at $\mathbf{x}_i$, Ω_{si} :i^{th} local domain, $\partial\Omega_{si}$:i^{th} local boundary, L_{sj} : non-intersecting part of $\partial\Omega_{sj}$, Γ_{sj} : intersecting part of , $\partial\Omega_{sj}=L_{sj}\cup\Gamma_{sj}$.

VII. VALIDATION PROCEDURE

Following the principal work of James Rautio [25], i.e., the convergence analysis, we designed a number of abstract problems. The MLBE is applied to each and the convergence of the solutions is investigated by convergence curves.

For error estimation, we use the relative error of energy defined as:

$$r_e = \|u - u_{exact}\| / \|u_{exact}\|. \quad (25)$$

with $\|u\| = 1/2\left(\int_\Omega |u|^2 \, d\Omega\right)^{1/2}$.

VIII. 2D EXAMPLES

In this section, 2D Laplace and Helmholtz equations with various boundary conditions are solved. We have divided these examples into two types; elementary and advanced. Elementary examples are rectangular with a well-behaved boundary conditions and smooth solutions. On the other hand, advanced examples are non-rectangular or with a singular boundary condition or have a more complex solution. Nodal spacing is expressed by $h_v, v = x, y$, in corresponding directions with $h = \left(h_x^2 + h_y^2\right)^{1/2}$. Unless otherwise stated, the problem domains are described by regular node arrangements with equal spacing. In addition, for all problems α_i and β_i are selected as mentioned in part III. Local domains are assumed rectangular for internal nodes. For boundary nodes, they are rectangular for straight and circular for curved parts of the main boundary. In all cases, the largest sides of the rectangles are denoted by *L* and the radii by *R*. Finally, the number integration points for Gauss-Legendre quadrature is indicated by N_{GL} .

A. Elementary examples

The domain of these examples is a 2×2 squares centered at the origin. The bottom, right, top, and left boundaries are named $\Gamma_1, \Gamma_2, \Gamma_3$ and Γ_4, respectively. For all Laplace problems, the exact solution is selected to be [21]:

$$u_{exact}^{Laplace} = -x^3 - y^3 + 3x^2 y + 3xy^2. \quad (26)$$

Similarly, for all Helmholtz problems:

$$u_{exact}^{Helmholtz} = \sin(2x)\sin\left(\sqrt{5}y\right). \quad (27)$$

The details of these problems and the figures containing the corresponding convergence curves are listed in Table 1. For all these examples $L \le 0.1h$ and $N_{GL} = 10$. To demonstrate that MLBE is an alternative to LBIE, all these examples are also solved by LBIE with the same discretization parameters.

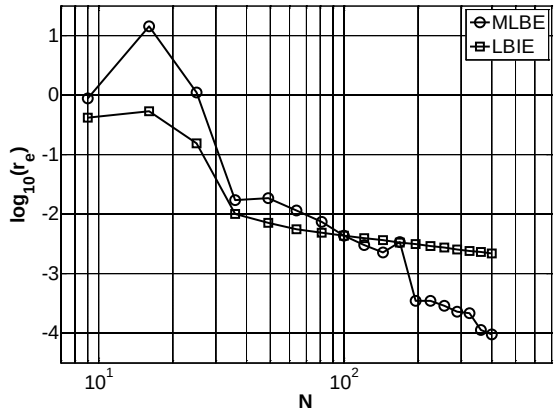

Fig. 2. Convergence of Laplace equation for (a) Dirichlet, (b) Dirichlet/Neumann and (c) Neumann boundary conditions.

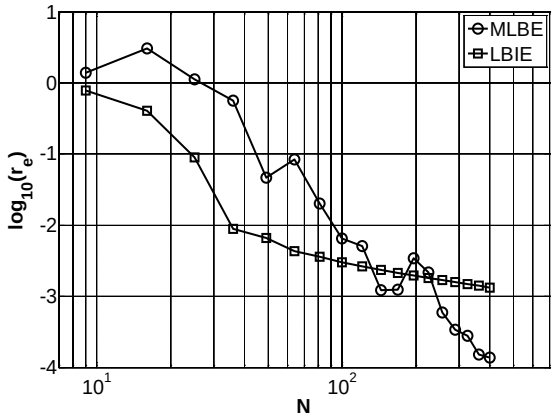

(a)

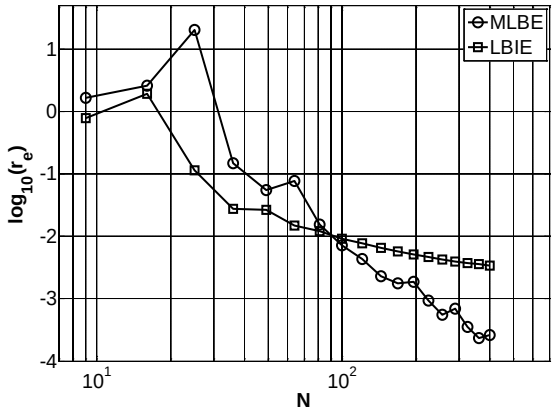

(b)

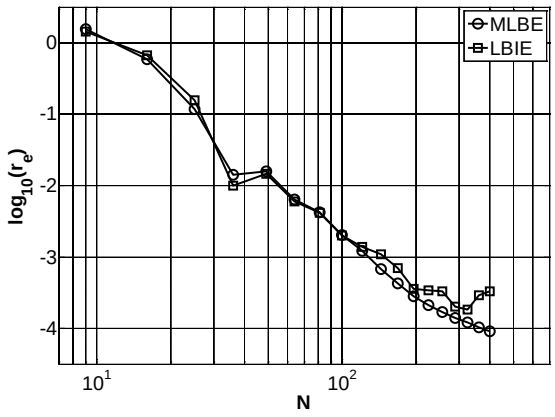

(c)

Fig. 3. Convergence of Helmholtz equation for (a) Dirichlet, (b) Dirichlet/Neumann and (c) Neumann boundary conditions.

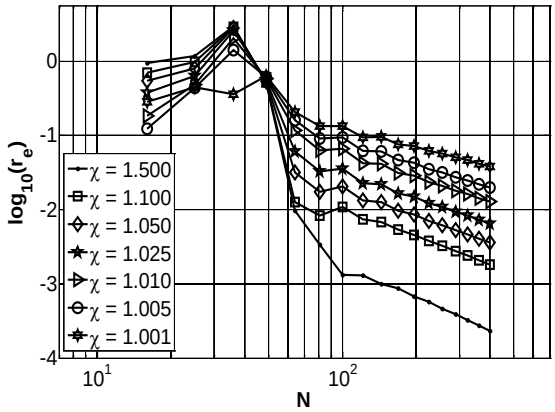

(a)

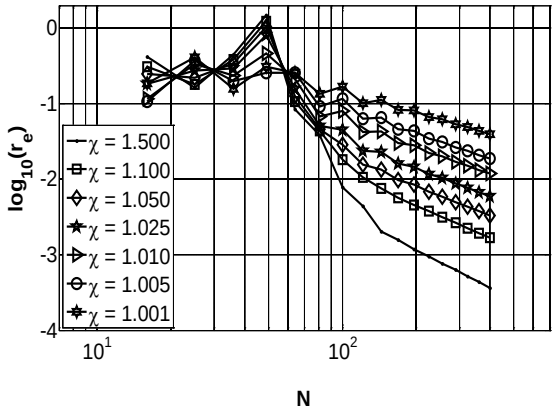

(b)

Fig. 4. Convergence of the first advanced example for (a) Laplace and (b) Helmholtz equation.

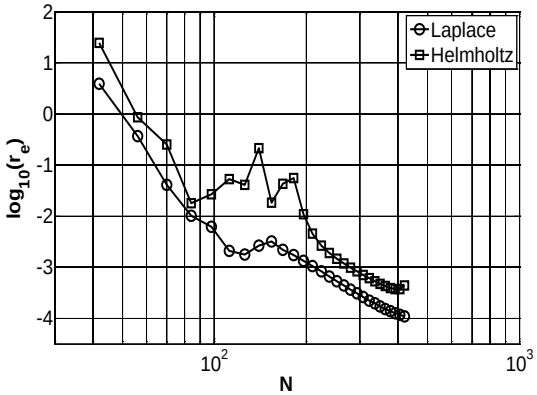

Fig. 5. Convergence curves of the second advanced example.

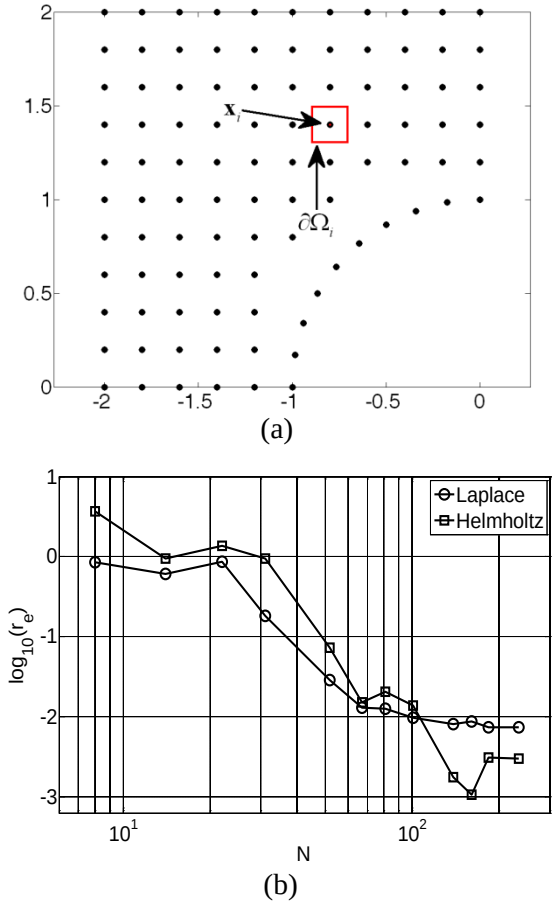

Fig. 6. (a) Nodal arrangement and the shape of a sample test domain and (b) convergence curves of the third advanced example.

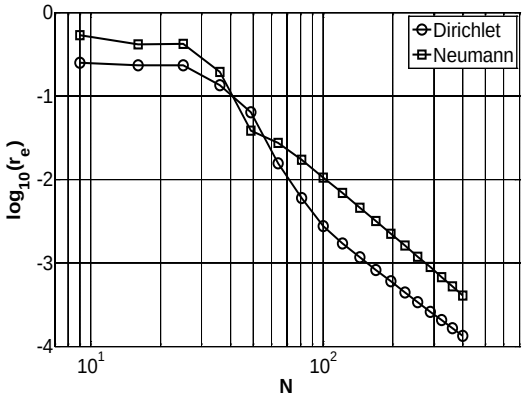

Fig. 7. Convergence of the sequence of the first nine eigenvalues for the last advanced example.

B. Advanced examples

The first of these examples has a domain similar to the elementary ones, but with singular Dirichlet boundary condition:

$$u(\mathbf{x}) = \left[\left(x^2 - \chi\right)\left(y^2 - \chi\right)\right]^{-1/2}, \mathbf{x} \in \partial\Omega. \quad (28)$$

where $\chi \in \{1.5, 1.1, 1.05, 1.025, 1.01, 1.005, 1.001\}$ and $k_0 = 3$ for Helmholtz equation. In this example, $L \le 0.001h$ and $N_{GL} = 3$. Convergence curves corresponding to solutions of Laplace and Helmholtz equations by the MLBE method are depicted in Fig. 4.

The domain of our second advanced example is a circular disc with inner and outer radii equal to $r_{\min} = 0.1$ and $r_{\max} = 1$, respectively. The exact solution for Laplace and Helmholtz equations are selected to be:

$$u_{exact}^{Laplace} = r^3 \cos(3\theta). \quad (29)$$

and

$$u_{exact}^{Helmholtz} = J_3(3r)\cos(3\theta). \quad (30)$$

Table 1: Mathematical statement of the elementary examples and address of the related convergence curves

Boundary conditions	Equation	
	Laplace	Helmholtz
$u(\Gamma_i) = \overline{u_i}, i = 1,2,3,4$	Fig. 2(a)	Fig. 3(a)
$\begin{cases} u(\Gamma_i) = \overline{u_i}, i = 1,3 \\ u_{,n}(\Gamma_i) = \overline{q_i}, i = 2,4 \end{cases}$	Fig. 2(b)	Fig. 3(b)
$u_{,n}(\Gamma_i) = \overline{q_i}, i = 1,2,3,4$	Fig. 2(c)	Fig. 3(c)

In addition, the boundary condition is selected to be Dirichlet. This example has two important features. First, its geometry is not Cartesian. Second, since its boundary condition is all Dirichlet, it can validate the theoretical statements of the third section, i.e. the method is capable of imposing the essential boundary conditions on a curved boundary. Nodal arrangement for this example is polar with fixed 10 angular samples and radial samples increase from 3 to 20. For local domains, $L = 0.001h$ and $R = 0.001h$ are selected with $N_{GL} = 10$. Note that, although the spacing of nodes increases with radial distance, the size of local domains is fixed. In general, one can choose these sizes with respect to distance of each node from its neighbors. Since at any boundary node, either $\sin(\theta_i) \neq 0$ or $\cos(\theta_i) \neq 0$, imposition of the Dirichlet boundary condition at each node *i* on the boundary is guaranteed by:

$$\begin{cases} \sin(\theta_i)=0 \Rightarrow \alpha_i=\cos(\theta_i)^{-1},\ \beta_i=0 \\ \cos(\theta_i)=0 \Rightarrow \alpha_i=0,\ \beta_i=\sin(\theta_i)^{-1} \\ \sin(2\theta_i)\neq 0 \Rightarrow \alpha_i=2^{-1}\cos(\theta_i)^{-1},\ \beta_i=2^{-1}\sin(\theta_i)^{-1} \end{cases} \tag{31}$$

for Laplace, and:

$$\begin{cases} \sin(\theta_i)=0 \Rightarrow \begin{cases} \alpha_i=2^{1/2}\cos(\theta_i)^{-1} \\ \beta_i=\left(k_0^2-\alpha_i^2\right)^{1/2} \end{cases} \\ \cos(\theta_i)=0 \Rightarrow \begin{cases} \alpha_i=\left(k_0^2-\beta_i^2\right)^{1/2} \\ \beta_i=2^{1/2}\sin(\theta_i)^{-1} \end{cases} \\ \sin(2\theta_i)\neq 0 \Rightarrow \begin{cases} \alpha_i=2^{1/2}\cos(\theta_i)+\left(k_0^2-2\right)^{1/2}\sin(\theta_i) \\ \beta_i=2^{1/2}\sin(\theta_i)-\left(k_0^2-2\right)^{1/2}\cos(\theta_i) \end{cases} \end{cases} . \tag{32}$$

for the Helmholtz equation. It is straightforward to see that such selections correspond to $w_{i,n}(\mathbf{x}_i)=1\neq 0$. One important point remains to be mentioned. In contrast to mesh/grid based methods that approximate curved boundaries with piecewise linear functions, in meshfree methods, it is possible to either move exactly on the boundary or to interpolate/approximate their curvature with proper shape functions [24]. In this example, the first choice was possible and is applied. Convergence curves are depicted in Fig. 5.

The third advanced example is devoted to a domain with irregular boundary. The nodal description of its geometry for a sample pass is shown in Fig. 6(a). Evidently, both the geometry and the nodal arrangement are irregular. The exact solution for Laplace and Helmholtz equations are selected the same as the elementary examples with the following mixed boundary conditions:

$$\begin{cases} \textit{Neumann},\ x=0 \\ \textit{Dirichlet},\ \textit{otherwise} \end{cases}. \tag{33}$$

Solution parameters are the same as the previous example except the number of quadrature points is reduced to 3. Convergence curves are depicted in Fig. 6(b). As a final 2D example, the Helmholtz eigenvalue problem is solved over a square domain of unit side length. The convergence analysis is based on the sequence of the first nine eigenvalues. The corresponding convergence curves for all-Neumann and all-Dirichlet homogeneous boundary conditions are depicted in Fig. 7. For this problem $L\leq 0.4h$ and $N_{GL}=10$.

IX. APPLICATION TO 3D VECTOR WAVE EQUATION

In this section, we extend the use of the MLBE method to a highly complicated equation; e.g., the 3D vector wave equation:

$$\begin{cases} \nabla\times\nabla\times\mathbf{U}(\mathbf{r})-k_0^2\mathbf{U}(\mathbf{r})=0,\ \mathbf{r}\in V \\ \mathbf{n}\times\mathbf{U}(\mathbf{r})=\overline{\mathbf{U}},\ \mathbf{r}\in S_U \\ \mathbf{n}\times\nabla\times\mathbf{U}(\mathbf{r})=\overline{\mathbf{Q}},\ \mathbf{r}\in S_Q \end{cases} \tag{34}$$

where V is the volume bounded by $S=S_U\cup S_Q$ and $\mathbf{n}$ the unit normal to S [23]. Suppose the vector function $\mathbf{w}$ is a proper homogeneous solution of the vector wave equation. Following the vectorial equivalent steps of Section II,

$$\begin{aligned} &\int_{S_U}(\mathbf{w}\times\mathbf{n})\cdot(\nabla\times\mathbf{U})\,dS+\int_{S_Q}(\mathbf{n}\times\mathbf{U})\cdot(\nabla\times\mathbf{w})\,dS \\ &=-\int_{S_U}\overline{\mathbf{U}}\cdot(\nabla\times\mathbf{w})\,dS-\int_{S_Q}\mathbf{w}\cdot\overline{\mathbf{Q}}\cdot dS+\int_V\mathbf{w}\cdot\mathbf{P}\cdot dV. \end{aligned} \tag{35}$$

The next step is finding a proper $\mathbf{w}$, which for the ith node should satisfy:

$$\begin{cases} \nabla\times\nabla\times\mathbf{w}_i(\mathbf{r})-k_0^2\mathbf{w}_i(\mathbf{r})=0 \\ \mathbf{w}_i(\mathbf{r})\neq 0,\ \mathbf{r}_i\in S_Q \\ \nabla\times\mathbf{w}_i(\mathbf{r})\neq 0,\ \mathbf{r}_i\in S_U \end{cases} \tag{36}$$

Since (34) is a vector equation, we need three linearly independent proper vector weights. Making use of electromagnetic potentials, it is straightforward to show that for the i^{th} node, the following is a set of proper homogeneous solutions:

$$\begin{cases} \mathbf{w}_{i1}(\mathbf{x}+\mathbf{x}_i)=\sin(\alpha_{i1}x+\beta_{i1}y+\gamma_{i1}z+\pi/4) \\ \qquad\times\left(\alpha_{i1}^2-k_0^2,\ \alpha_{i1}\beta_{i1},\ \alpha_{i1}\gamma_{i1}\right) \\ \mathbf{w}_{i2}(\mathbf{x}+\mathbf{x}_i)=\sin(\alpha_{i2}x+\beta_{i2}y+\gamma_{i2}z+\pi/4) \\ \qquad\times\left(\alpha_{i2}\beta_{i2},\ \beta_{i2}^2-k_0^2,\ \beta_{i2}\gamma_{i2}\right) \\ \mathbf{w}_{i3}(\mathbf{x}+\mathbf{x}_i)=\sin(\alpha_{i3}x+\beta_{i3}y+\gamma_{i3}z+\pi/4) \\ \qquad\times\left(\alpha_{i3}\gamma_{i3},\ \beta_{i3}\gamma_{i3},\ \gamma_{i3}^2-k_0^2\right) \\ \alpha_{ij}^2+\beta_{ij}^2+\gamma_{ij}^2=k_0^2,\ j=1,2,3 \end{cases} . \tag{37}$$

where α_{ij}, β_{ij} and γ_{ij} are non-zero constant scalars, provided that they are selected such that linear independency is assured. The reason for introducing the aforementioned parameters is similar to statements of Section III. Now, consider three scenarios of Cartesian coordinate problems. The most symmetric selection is linear dependent and makes the coefficient matrix unsolvable. One choice that leads to satisfactory results is:

$$\begin{cases} \alpha_{i1} = -k_0/\sqrt{3},\ \beta_{i1} = k_0/\sqrt{3},\ \gamma_{i1} = k_0/\sqrt{3} \\ \alpha_{i2} = k_0/\sqrt{3},\ \beta_{i2} = -k_0/\sqrt{3},\ \gamma_{i2} = k_0/\sqrt{3}. \\ \alpha_{i3} = k_0/\sqrt{3},\ \beta_{i3} = k_0/\sqrt{3},\ \gamma_{i3} = -k_0/\sqrt{3} \end{cases} \quad (38)$$

There exists another choice that can be regarded as a trivial solution:

$$\begin{cases} \alpha_{i1} = 0,\ \beta_{i1} = k_0/\sqrt{2},\ \gamma_{i1} = k_0/\sqrt{2} \\ \alpha_{i2} = k_0/\sqrt{2},\ \beta_{i2} = 0,\ \gamma_{i2} = k_0/\sqrt{2}. \\ \alpha_{i3} = k_0/\sqrt{2},\ \beta_{i3} = k_0/\sqrt{2},\ \gamma_{i3} = 0 \end{cases} \quad (39)$$

Although this set of functions is linear independent, it is not reliable. A comparison between the weighting functions sets (38) and (39) will be made in what follows. To numerically verify the validity of the aforementioned analytical expressions, we first apply it to a rectangular block of $1.0\lambda_0 \times 1.0\lambda_0 \times 0.1\lambda_0$, $-l \le x, y \le l, 0 \le z \le t$ and singular Dirichlet boundary condition. The exact solution is selected to be:

$$\begin{aligned} \mathbf{U}_I = {} & \hat{\mathbf{x}} \sin\left[k_0 (y+z)/\sqrt{2} + \pi/4\right] \\ & + \hat{\mathbf{y}} \sin\left[k_0 (x+z)/\sqrt{2} + \pi/4\right] \\ & + \hat{\mathbf{z}} \sin\left[k_0 (x+y)/\sqrt{2} + \pi/4\right], \mathbf{r} \in \Omega. \end{aligned} \quad (40)$$

subject to:

$$\begin{aligned} \mathbf{U}_B = {} & \hat{\mathbf{x}} \sin\left[k_0 (y+z)/\sqrt{2} + \pi/4\right] \\ & + \hat{\mathbf{y}} \sin\left[k_0 (x+z)/\sqrt{2} + \pi/4\right] \\ & + \hat{\mathbf{z}} \frac{\sin\left[k_0 (x+y)/\sqrt{2} + \pi/4\right]}{\sqrt{\left|x^2 - (\chi l)^2\right| + \left|y^2 - (\chi l)^2\right| + \left|z - (\chi t)\right|^2}}, \mathbf{r} \in \partial\Omega \end{aligned} \quad (41)$$

where $\chi \in \{1.5, 1.1, 1.05, 1.025, 1.01, 1.005, 1.001\}$. For this problem, we have hybridized the MLBE and the meshfree collocation methods [26]. The later is applied to all boundaries except the top one and the former to other nodes. This is simply done by switching to Dirac delta as weight function for the nodes to be solved by the collocation method. In harmony with the problem domain, the local domains for internal and top-boundary nodes are selected to be $L_x \times L_y \times L_z$ rectangular blocks with $L_x \le 0.3h$, $L_y \le 0.3h$ and $L_z \le 0.03h$ where $h = \left(h_x^2 + h_y^2 + h_z^2\right)^{1/2}$. For numerical integration over each surface, $N_{GL} = 9$ is used. Since the rest of the nodes are solved by the collocation method, the concept of local domain is inapplicable. Equation set (38) is used as weight function. The convergence of the electric field is depicted in Fig. 8(a). For comparison, this example is also solved by equation set (39) with $\chi = 0.001$ as depicted in Fig. 8(b). Definitely, solution parameters are the same.

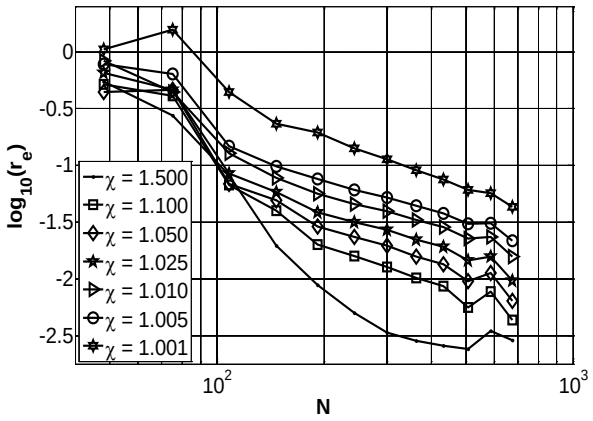

(a)

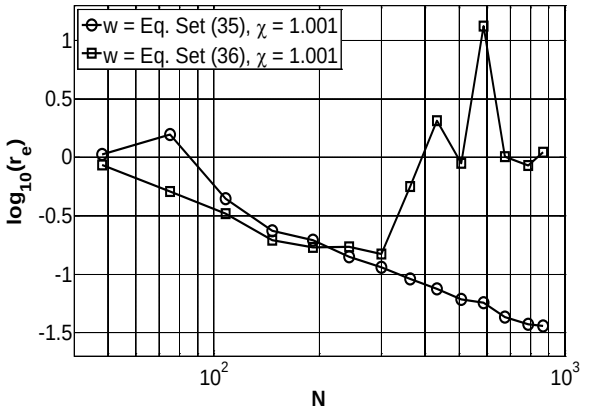

(b)

Fig. 8. Convergence of the problem corresponding to 3D vector wave equation over a rectangular block by (a) equation set (35) and (b) equation set (35) and (36) as weighting.

X. CONCLUSION

It is shown that the MLBE method is a good candidate for the numerical solution of PDEs. Comparison with the LBIE method also shows better convergence in the limit. The main advantage of the MLBE method over the LBIE method is the absence of singular integrands.

ACKNOWLEDGMENT

The authors appreciate Prof. M. Dehghan for inputs in meshfree methods, and Prof. R. F. Dana, for inputs regarding validation techniques.

REFERENCES

[1] Y. Marechal, "Some Meshless Methods for Electromagnetic Field Computations," *IEEE Trans. Magn.*, vol. 34, no. 5, pp. 3351-3354, 1998.

[2] C. Herault and Y. Marechal, "Boundary and Interface Conditions in Meshless Methods," *IEEE Trans. Magn.*, vol. 35, no. 3, pp. 1450-1453, 1999.

[3] S. L. Ho, S. Yang, J. M. Machado, and H. C. Wong, "Application of a Meshless Method in Electromagnetics," *IEEE Trans. Magn.*, vol. 37, no. 5, pp. 3198-3201, 2001.

[4] L. Xuan, Z. Zeng, B. Shanker, and L. Udpa, "Meshless Method for Numerical Modeling of Pulsed Eddy Currents," *IEEE Trans. Magn.*, vol. 40, no. 6, pp. 3457-3462, 2004.

[5] S. L. Ho, S. S. Yang, H. C. Wong, and G. Ni, "Meshless Collocation Method Based on Radial Basis Functions and Wavelets," *IEEE Trans. Magn.*, vol. 40, no. 2, pp. 1021-1024, 2004.

[6] S. L. Ho, S. S. Yang, G. Ni , H. C. Wong, and Y. Wang, "Numerical Analysis of Thin Skin Depths of 3-D Eddy-Current Problems using a Combination of Finite Element and Meshless Methods," *IEEE Trans. Magn.*, vol. 40, no. 2, pp. 1354-1357, 2004.

[7] S. L. Ho, S. S. Yang, H. C. Wong, E. W. C. Lo and G. Ni, "Refinement Computations of Electromagnetic Fields using FE and Meshless Methods," *IEEE Trans. Magn.*, vol. 41, no. 5, pp. 1456-1459, 2005.

[8] Y. Zhang, K. R. Shao, D. X. Xie and J. D. Lavers, "Meshless Method Based on Orthogonal Basis for Electromagnetics," *IEEE Trans. Magn.*, vol. 41, no. 5, pp. 1432-1435, 2005.

[9] Q. Li and K. Lee, "Adaptive Meshless Method for Magnetic Field Computation," *IEEE Trans. Magn.*, vol. 42, no. 8, pp. 1996-2003, 2006.

[10] R. K. Gordon and W. E. Hutchcraft, "The Use of Multiquadric Radial Basis Functions in Open Region Problems," *Applied Computational Electromagnetics Society (ACES) Journal*, vol. 21, no. 2, pp. 127-134, July 2006.

[11] Y. Zhang, K. R. Shao, J. Zhu, D. X. Xie, and J. D. Lavers, "A Comparison of Point Interpolative Boundary Meshless Method Based on PBF and RBF for Transient Eddy-Current Analysis," *IEEE Trans. Magn.*, vol. 43, no. 4, pp. 1497-1500, 2007.

[12] F. G. Guimaraes, R. R. Saldanha, R. C. Mesquita, D. A. Lowther, and J. A. Ramirez, "A Meshless Method for Electromagnetic Field Computation Based on the Multiquadratic Technique," *IEEE Trans. Magn.*, vol. 43, no. 4, pp. 1281-1284, 2007.

[13] S. Ikuno, K. Takakura, and A. Kamitani, "Influence of Method for Imposing Essential Boundary Condition on Meshless Galerkin/Petrov-Galerkin Approaches," *IEEE Trans. Magn.*, vol. 43, no. 4, pp. 1501-1504, 2007.

[14] S. McFee, D. Ma, and M. Golshayan, "A Parallel Meshless Formulation for H-P Adaptive Finite Element Analysis," *IEEE Trans. Magn.*, vol. 44, no. 6, pp. 786-789, 2008.

[15] T. Kaufmann, C. Fumeaux, and R. Vahldieck, "The Meshless Radial Point Interpolation Method for Time-Domain Electromagnetics", *IEEE MTT-S Int. Microwave Symp. Dig.*, Atlanta, pp. 61-64, 2008.

[16] Y. Yu and Z. Chen, "A 3-D Radial Point Interpolation Method for Meshless Time-Domain Modeling," *IEEE Trans. Microwave Theory Tech.*, vol. 57, no. 8, pp. 2015-202, 2009.

[17] Y. Yu and Z. Chen, "Towards the Development of an Unconditionally Stable Time-Domain Meshless Method," *IEEE Trans. Microwave Theory Tech.*, vol. 58, no. 3, pp. 578-586, 2010.

[18] T. Kaufmann, C. Engström, C. Fumeaux, and R. Vahldieck, "Eigenvalue Analysis and Longtime Stability of Resonant Structures for the Meshless Radial Point Interpolation Method in Time Domain", *IEEE Trans. Microwave Theory Tech*., vol. 58, no. 12, pp. 3399-3408, 2010.

[19] R. D. Soares, R. C. Mesquita, F. J. S. Moreira, "Axisymmetric Electromagnetic Resonant Cavity Solution by a Meshless Local Petrov-Galerkin Method," *Applied Computational Electromagnetics Society (ACES) Journal*, vol. 26, no. 10, pp. 792-799, October 2011.

[20] S. N. Atluri and T. A. Zhu, "A New Meshless Local Petrov-Galerkin MLPG) Approach in Computational Mechanics," *CMES*, vol. 22, pp.117-127, 1998.

[21] T. Zhu, J.-D. Zhang, and S. N. Atluri, "A Local Boundary Integral Equation (LBIE) Method in Computational Mechanics, and a Meshless Discretization Approach," *CMES*, vol. 3, no.1, pp. 223-235, 1998.

[22] J. G. Wang and G. R. Liu, "Radial Point Interpolation Method for Elastoplastic Problems," presented at 1st *Int. Conf. Structural Stability and Dynamics*, Taipei, Taiwan, 2000.

[23] J. Jin, *The Finite Element Method in Electromagnetics*, Second Edition. John Wiley & Sons, 2002.

[24] G. R. Liu, *Mesh Free Methods*, CRC Press, 2003.

[25] J. C. Rautio, "The Microwave Point of View on Software Validation," *IEEE Antennas Propagat. Mag.*, vol. 38, no. 2, pp. 68-71, 1996.

[26] G. R. Liu and Y. T. Gu, *An Introduction to MeshFree Methods and Their Programming*, Springer, 2005.

Babak Honarbakhsh was born in Tehran, Iran. He received his B.S. and M.S. degrees in Electrical Engineering from Amirkabir University of Technology where he is currently working toward his Ph.D. degree. His current research interest is numerical solution of electromagnetic problems by meshfree methods.

Ahad Tavakoli was born in Tehran, Iran on March8, 1959. He received the B.S. and M.S. degrees from the University of Kansas, Lawrence, and the Ph.D. degree from the University of Michigan, Ann Arbor, all in Electrical Engineering, in 1982, 1984, and 1991, respectively.

In 1991, he joined the Amirkabir University of Technology, Tehran, Iran where he is currently a Professor in the Department of Electrical Engineering. His research interests include EMC, scattering of electromagnetic waves and microstrip antennas.